Binding Domain of Human Parathyroid Hormone Receptor: From Conformation to Function[†,‡]

Maria Pellegrini,[§] Alessandro Bisello,[||] Michael Rosenblatt,[||] Michael Chorev,[||] and Dale F. Mierke*[,§]

Department of Molecular Pharmacology, Physiology, & Biotechnology, Division of Biology & Medicine, and Department of Chemistry, Brown University, Providence, Rhode Island 02912, and Division of Bone and Mineral Metabolism, Charles A. Dana & Thorndike Laboratories, Department of Medicine, Beth Israel Deaconess Medical Center, Harvard Medical School, 330 Brookline Ave., Boston, Massachusetts, 02215

Received May 27, 1998; Revised Manuscript Received July 23, 1998

ABSTRACT: A 31 amino acid fragment of the extracellular N-terminus of the human G-protein coupled receptor for parathyroid hormone (PTH1R) has been structurally characterized by NMR and molecular dynamics simulations. The fragment PTH1R[168−198] includes residues 173−189, shown by photoaffinity cross-linking to be a contact domain with position 13 of parathyroid hormone (PTH). The structure of PTH1R[168−198], determined in a micellar solution of dodecylphosphocholine to mimic the membrane environment, consists of three α-helices, separated by a well-defined turn and a flexible region. The topological orientation of PTH1R[168−198] was determined from nitroxide-radical induced relaxation of NMR signals utilizing 5- and 16-doxylstearic acid. The C-terminal helix (residues 190−196), consisting of seven amino acids of the first transmembrane domain, is very hydrophobic and embedded in the lipid core. This helix is preceded by a well-defined turn, forming an approximate 90° bend, placing the other helices (residues 169−176 and 180−189), both of which are amphipathic, on the surface of the micelle. In this orientation, many hydrophilic residues of the receptor, including Glu^{177}, Arg^{179}, Arg^{181}, Glu^{182}, Asp^{185}, and Arg^{186}, are projecting toward the solvent available to form complementary Coulombic interactions with the polar residues of the principal binding domain of the ligand (e.g., Arg^{25}, Lys^{26}, Lys^{27}, Asp^{30}, and His^{32}). Given that the binding domain of PTH adopts an amphipathic α-helix which lies on the membrane, we visualize ligand binding as a two stage process involving a nonspecific hydrophobic interaction of amphipathic helices with the membrane, followed by two-dimensional diffusion leading to highly specific, ligand−receptor interaction.

Parathyroid hormone (PTH)[1] is the principal regulator of calcium and phosphate ion homeostasis. PTH is active through a G-protein coupled receptor (PTH1R) (*1*, *2*) affecting two intracellular signaling pathways: adenylyl cyclase/cAMP/protein kinase A and inositol triphosphate/cytosolic calcium/protein kinase C. PTH1R belongs to a subfamily of G-protein coupled receptors, presumed to exhibit the characteristic seven membrane-spanning helices as in rhodopsin, sharing a long amino-terminal extracellular region, multiple glycosylation sites, and eight conserved extracellular cysteine residues (*3*). Recent mutational and chimera studies of PTH1R indicate that the extracellular, amino-terminus constitutes one of the sites for ligand/receptor interaction (*4*−*6*). Studies of the ligand have shown that the N-terminal 1−34 fragment of the hormone, PTH[1−34], is equipotent to native PTH and that residues 25−34 constitute the principal binding domain (*7*, *8*).

Recent photoaffinity cross-linking experiments have directly identified a contact between position 13 of PTH and a domain comprising residues 173−189 of the N-terminus of PTH1R, adjacent to the putative first transmembrane helix (TM1) (*9*). To obtain structural insight into the interaction between the receptor and ligand, we have undertaken the investigation of the conformational propensities of both. The NMR-derived structures of human PTH(1−34) in a membrane mimetic show a well-defined amphipathic α-helix for the C-terminal binding domain (*10*). Molecular modeling of human PTH1R, based on the rhodopsin/bacteriorhodopsin structure (*11*, *12*) and homology analysis (*13*), suggested that the contact domain, PTH1R[173−189], adopts an amphipathic α-helix (unpublished data). On the basis of this, one may postulate complementary helix−helix interactions as one

[†] This work was supported, in part, by Grants R29-GM54082 (to D.F.M.) and R01-DK47940 (to M.R.) from the National Institutes of Health.

[‡] The structure coordinates have been deposited in the Brookhaven Protein Data Bank (filename 1BL1).

* To whom correspondence should be addressed. Phone: (401) 863-2139. Fax: (401) 863-1595. E-mail: Dale_Mierke@Brown.edu.

[§] Brown University.

[||] Harvard Medical School.

[1] Abbreviations: doxyl, 4,4-dimethyl-3-oxazolidinyloxy; DG, distance geometry; G-Protein, guanine nucleotide-binding regulatory protein; MD, molecular dynamics; NMR, nuclear magnetic resonance; NOE, nuclear Overhauser enhancements; PTH, human parathyroid hormone; PTHrP, parathyroid hormone-related protein; PTH1R, parathyroid hormone receptor 1; ROESY, rotational-Overhauser enhancement spectroscopy; DPC, dodecylphosphocholine; TM, transmembrane; TOCSY, total-correlation spectroscopy; DQF-COSY, double quantum filtered correlation spectroscopy, NOESY, nuclear Overhauser enhancement spectroscopy.

S0006-2960(98)01265-3 CCC: $15.00
Published on Web 08/22/1998

of the elements in ligand−receptor recognition and binding. To test this hypothesis, we have examined the conformational characteristics of PTH1R[168−198] in the presence of dodecylphosphocholine micelles by NMR and distance geometry (DG) calculations. We subsequently incorporated free radical bearing fatty acids in the micelles to explore (by NMR) the orientation of the peptide relative to the membrane mimetic. Extensive molecular dynamics (MD) calculations, utilizing a decane/water simulation cell (*14*), have been carried out to obtain the final, refined structures and to describe the partition behavior of the molecule between the two solvents. From the inspection of the high-resolution structure of PTH1R[168−198], the specific amino acids of the receptor in this contact domain available for interaction with the ligand have been identified.

EXPERIMENTAL PROCEDURES

Peptide Synthesis. The peptide, Ac−SEAVKFLTNETR-EREVFDRLGMIYTVGYSVC−NH_2, PTH1R[168−198], was synthesized by solid-phase methodology with an Applied Biosystems 430A peptide synthesizer as described (*15*). The purity was established by analytical high-performance liquid chromatography and the structural integrity by amino acid analysis and electron-spray mass spectrometry.

NMR Methods. PTH1R[168−198] was examined in aqueous solution (ca. 2.4 mM, 9:1 $H_2O/^2H_2O$, pH 4.5 not corrected), in the presence of 150 mM dodecylphosphocholine-d_{38} (DPC). All of the experiments were recorded on a Varian Unity 500 spectrometer at temperatures varying between 298 and 318 K. Data processing utilized Varian software (VNMR) or *Felix* (Biosym/MSI, San Diego). Chemical shifts were referenced to the signal of tetramethylsilane (0.0 ppm).

The amino acid spin systems were identified from DQF−COSY (*16*) and TOCSY (*17*, *18*) spectra. NOESY (*19*, *20*) experiments with mixing times of 125−350 ms were employed for the sequential assignment. The TOCSY utilized a MLEV-17 sequence to realize mixing times of 35−70 ms with a spin-lock field of 10 000 Hz. Suppression of the solvent signal was achieved by continuous wave presaturation at low power during the relaxation delay (1.5−2 s). The NOESY experiments utilized additional presaturation during the mixing time, or alternatively, coupled a "jump and return" observation pulse (*21*) with 0.4 s of presaturation. The typical spectral width was 5000 Hz in both dimensions, with 4096 data points in t_2 and 320−512 data points in t_1 and with 32−128 scans at each increment. Forward linear prediction to 1024 points was applied to the incremented dimension; both dimensions were multiplied by Gaussian or shifted squared sine bell apodization functions, prior to Fourier transformation.

Radical-Induced Relaxation. The 5- and 16-doxylstearic acid were solubilized in methanol-d_4 to a final concentration of 53 mM. Aliquots of this solution were added to the solution of peptide and DPC to obtain 0.25−0.94 mM concentrations of the spin-label. The titrations with 5- and 16-doxylstearic acid were carried out separately on two equivalent peptide solutions. TOCSY experiments (mixing time 35 ms) were recorded under identical conditions before and after the addition of the doxylstearic acid. The intensities of cross-peaks involving both backbone (H^N-H^α) and side chain protons ($H^\alpha-H^\beta$, $H^\gamma-H^\delta$) were compared.

Distance Geometry. NOESY spectra acquired at 298, 308, and 318 K with a mixing time of 150 ms (with 10% randomization) were utilized to measure cross-peaks volumes. The volumes were converted to distances using the two-spin approximation. The resolved cross-peak between two protons within the α-helical domain of the peptide was utilized as a reference (Phe^{184} H^N-Asp^{185} H^N, 2.8 Å) (*22*, *23*). Addition and subtraction of 10% to the calculated distances yielded upper and lower bounds. Pseudoatom corrections were applied to methyl groups and methylene protons with coincident chemical shifts (*22*); the floating chirality approach (*24*) was utilized for nonstereospecifically assigned, resolved methylene protons. A home-written program was utilized to calculate an ensemble of structures fulfilling holonomic (constitutional) and experimental (proton−proton distances) restraints. The two-step procedure utilizes the random metrization algorithm (*25*) followed by optimization via conjugate gradients (*26*), and by distance driven dynamics (DDD) (*27*, *28*). The procedure is repeated first in four dimensions, for optimal sampling of the conformational space, and then in three dimensions. The final DDD on the 98 calculated structures was carried out at 500 K for 200 ps, followed by slow cooling to 0 K.

Molecular Dynamics. MD simulations were performed with GROMACS, version 1.6 (*29*). Interactive modeling utilized *Insight II* (Biosym/MSI, San Diego). To produce a solvent system consistent with the experimental conditions (water and DPC micelles) and acceptable computation times on standard workstations, a two-phase box of water and decane was implemented. A detailed description of the decane/water interface has appeared (*14*). All atoms were treated explicitly except for the CH_n atoms of the decane molecules which were treated as united atoms. For the dihedral angles $CH_2CH_2CH_2CH_2$ and $CH_2CH_2CH_2CH_3$ of decane, the Ryckaert-Bellemans potential was used (*14*, *30*). The single-point-charge (SPC) model was adopted for water (*31*, *32*). Initially a layer of decane was created, containing 100 molecules in the all-trans configuration and with parallel head-to-tail axes. This box underwent energy minimization for 200 steps (steepest descent) and 100 ps of molecular dynamics at 300 K, with a time constant of 2 fs. A twin-range cutoff for nonbonded forces of 0.8/1.0 nm was used; the pair list and forces for the range 0.8−1.0 nm were updated every 10 steps. A second layer of water was added utilizing a cubic box of 216 equilibrated SPC water molecules. The water molecules were allowed to keep a minimum distance of 0.23 nm from the atoms of the decane molecules. The two-phase cell, of dimensions 4.7 × 4.7 × 4.7 nm, underwent energy minimization and MD utilizing the conditions described above. The final cell was utilized to soak PTH1R[168−198].

One of the low-violation DG structures was used as the starting structure for the MD simulation. The molecule was placed in the (periodic) two-phase box of H_2O/decane, containing 992 water and 123 decane molecules in a volume of 101.6 nm^3. The charges of ionizable groups correspond to the pH of the NMR solution; no counterions were included. The system was energy minimized for 100 steps (steepest descent). In the following 10 ps of MD at 300 K (*33*), the peptide was restrained to its original position with

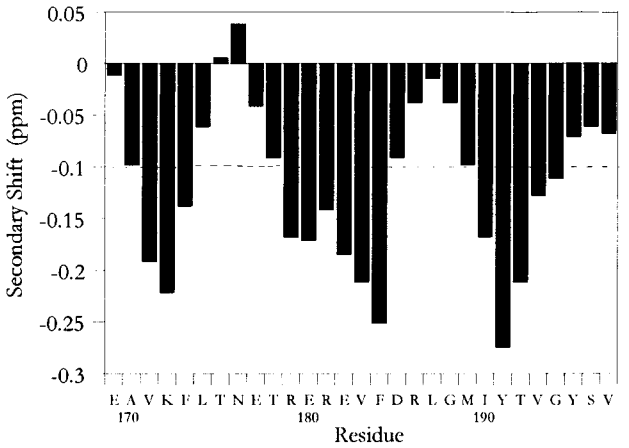

FIGURE 1: The secondary shifts of the α-protons of PTH1R[168−198] in aqueous solution (2.4 mM, pH 4.5) in the presence of DPC (150 mM) micelles.

a force constant of 1000 kJ mol^{-1} nm^{-1}. Experimental distance restraints were then introduced with a force constant of 10 000 kJ mol^{-1} nm^{-1} for the 400 ps of the simulation. Structures were sampled every 0.5 ps. One iteration took approximately 0.52 s on a SGI O2 (R5000, 200 MHz). The resulting trajectories were examined with analysis programs in the GROMACS package and home-written Fortran programs.

RESULTS

PTH1R[168−198] contains the 17 amino acid contact domain (residues 173−189) previously identified to cross-link to position 13 of PTH[1−34] (*9*). This contact domain was extended by nine amino acids at the C-terminus to include the hydrophobic residues postulated to be the beginning of TM1. These residues were included to anchor and orient the receptor fragment into the micelle. The dodecylphosphocholine micelles, utilized to mimic the membrane environment in the NMR studies, were also required for solubilization. In benign aqueous solution, the peptide formed a semisolid gel in approximately 20 min, which could not be resolubilized by variation of pH or ionic strength. Furthermore the DPC micelles provide a charged, zwitterionic interface and a hydrophobic core, properties of the biological membrane in which the receptor is located. Additionally, the micelle undergoes rapid reorientation in solution allowing for high-resolution NMR studies. The concentration of the DPC was adjusted to ensure more than one micelle per each peptide molecule (*34*, *35*).

Secondary Structure. The secondary shifts for H^{α} were calculated by subtracting the chemical shifts for unstructured peptides (*22*) from the experimentally measured chemical shifts and averaging the values over succeeding triplets of amino acids (*35*). The negative values observed for Ala^{170}−Leu^{174}, Thr^{178}−Asp^{185}, and Met^{189}−Tyr^{195} (Figure 1) are consistent with α-helical structure (*36*). At two positions along the sequence (in addition to the peptide termini), the H^{α} chemical shifts adopt random-coil values, indicating interruptions in the helical structure around residues Thr^{175} and Leu^{187}. The relevant nonsequential NOEs are reported in Figure 2. A series of correlations of type H^{N}_{i} to H^{N}_{i+1} or H^{N}_{i+2} and H^{α}_{i} to H^{N}_{i+3} or H^{N}_{i+4} confirms the presence of the three α-helical regions. In addition, strong NOEs of type H^{α}_{i} to H^{N}_{i+2} between Thr^{175}−Glu^{177} and Arg^{186}−Gly^{188} suggest the presence of turns.

A total of 83 structures were obtained from the DG calculations, with small penalty functions and no NOE violation. The structures converge to fairly regular α-helical segments encompassing residues 169−176, 181−189, and 192−195. The dihedral angle order parameters for ϕ and ψ (data not shown) indicate a high degree of order in the regions 169−176 and 180−195. The high disorder at Thr^{178} prevents the assessment of a preferred orientation of the N-terminal helix relative to the rest of the molecule. This disorder may be caused by the lack of experimental restraints, resulting from spectral overlap, rather than conformational disorder or flexibility. From Arg^{179} to the C-terminus the DG structures can be described as two consecutive helices forming an angle of ca. 90° between their axes. Interestingly, both the extracellular helix and the turn separating it from TM1 were correctly predicted by homology modeling of PTH1R (unpublished data). The average pairwise root-mean-square deviation (RMSD) of the backbone atoms of the entire peptide over the 83 structures is 5.5 Å. The ordered regions are characterized by an RMSD of 0.78 Å for residues 169−176, 1.46 Å for the second helix (residues 180−189), and 1.06 Å for the residues of the putative TM1 (190−196). Thirty structures from the DG calculations are represented in Figure 3. The structures have been superimposed in the C-terminal region to illustrate the well-defined second and third helical domains as well as the turn between these domains. As discussed above, the N-terminal helix assumes a range of different orientations relative to the rest of the molecule.

Topological Orientation. The topological orientation of the peptide relative to the DPC micelle was determined by titration with 5- and 16-doxylstearic acid, carrying a nitroxide radical at positions 5 and 16, respectively. The doxylstearic acid readily incorporates into DPC micelles, placing the nitroxide radical at the same level as the phosphate headgroups (5-doxyl) or slightly off-center from the core of the micelle (16-doxyl) (*38*). Upon addition of the doxylstearic acid to the peptide solution, NMR signals in close proximity to the radical are significantly broadened (a small background broadening of all resonances is usually observed) (*38*−*40*).

In the presence of 5-doxylstearic acid, most of the residues show a reduced intensity, indicating that a majority of the amino acids are proximal to the charged membrane surface (Figure 4A). In particular, the N-terminal helix displays a periodicity that agrees with an α-helix lying on the surface (i.e., the residues projecting into the solution are distal from the nitroxide radical). The effect on the other two helices is less specific, consistent with an orientation in which the residues are partially embedded in the micelle. The titration with 16-doxylstearic acid, which places the nitroxide near the center of the micelle, is expected to significantly affect only those residues in the hydrophobic core. Indeed, a reduction of intensity greater than 25% was observed for residues from Thr^{192} to the C-terminus. Residues 183−191 were moderately affected, while the N-terminal residues displayed almost no variation (see Figure 4B).

Conformation and Partition Behavior from MD. The starting structure, generated from the DG calculations, was placed in the biphasic water/decane cell with an orientation

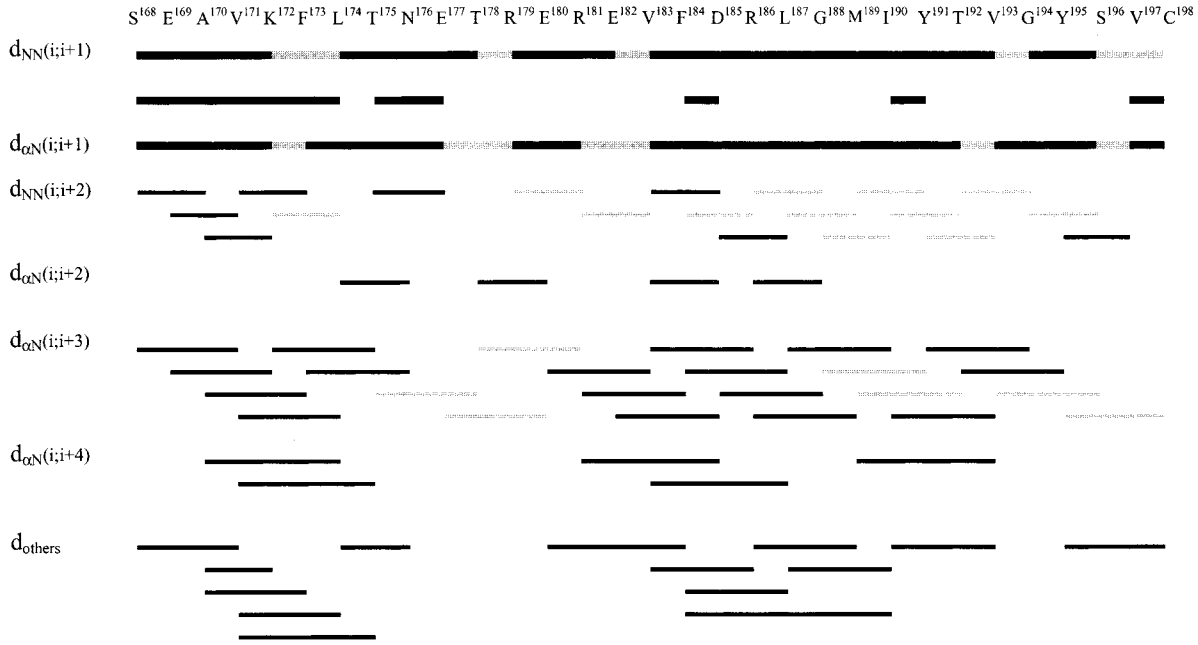

FIGURE 2: Relevant NOEs detected from NOESY spectra at 298, 308, and 318 K and utilized in the structure calculations. A shaded bar indicates a cross-peak not unambiguously identified due to resonance overlap.

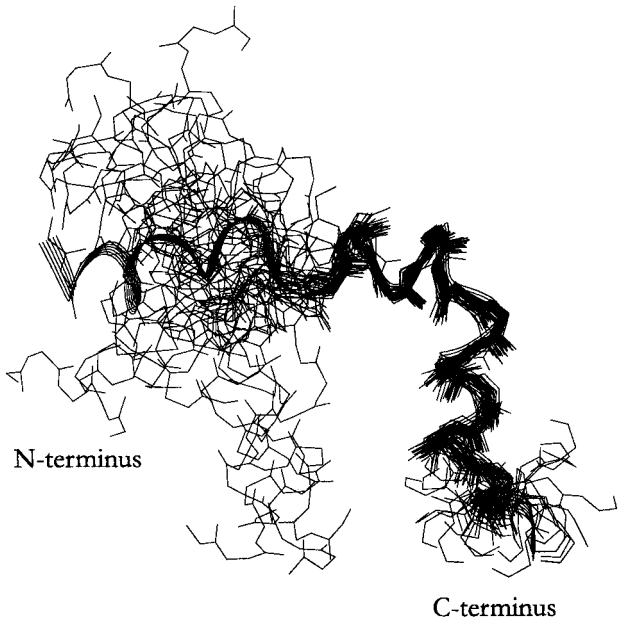

FIGURE 3: Backbone representation of 30 structures, with the backbone atoms of residues 180−198 superimposed, obtained from DG calculations.

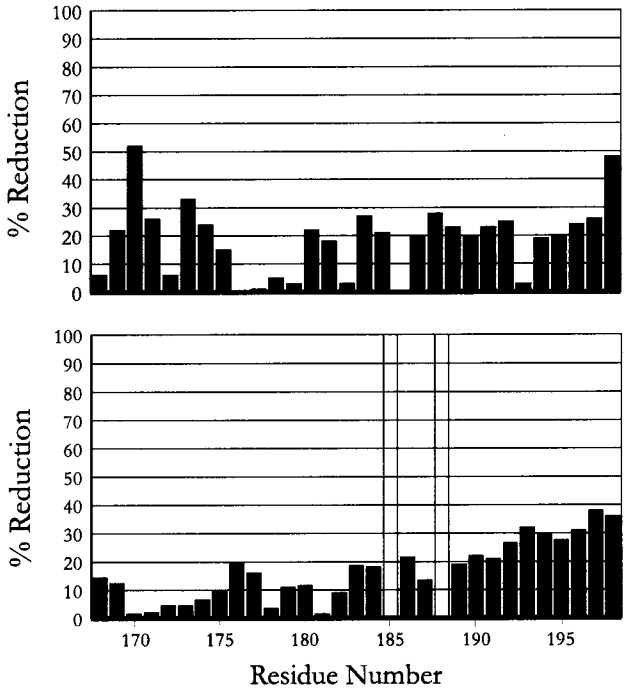

FIGURE 4: Histograms representing the reduction in cross-peak intensity for single residues (measured from TOCSY spectra) upon addition of 5-doxylstearic acid (top) or 16-doxylstearic acid (bottom). Empty bars indicate residues for which data could not be obtained.

based on the results of the NMR experiments in the presence of nitroxide radicals. The C-terminal helix (corresponding to the extracellular end of TM1), which was determined to be in the hydrophobic core of the micelle, was embedded in the decane phase with the helix axis perpendicular to the interface. This placed the other two helices at the interface, largely exposed to the water phase, in agreement with the results of the nitroxide-radical experiments. This orientation was maintained for the entire simulation (400 ps). The secondary structure and the tertiary arrangement of the three helices did not show significant changes, and no violation of the experimental distance restraints was observed (Figure 5). A second simulation was carried out to explore the most favorable partitioning of the peptide between the two media.

For this simulation, the peptide was placed entirely in the decane phase with the N-terminal helix directed away from the interface. During the first 70 ps of the simulation, the peptide translated and reoriented relative to the plane of the interface so that the N-terminal and middle helices reached the water phase, finally adopting the same orientation as obtained from the first simulation. No rearrangement of the secondary or tertiary structure was observed during this major redistribution of the molecule between the two solvents. The average backbone dihedral angles resulting from the MD simulation are reported in Table 1.

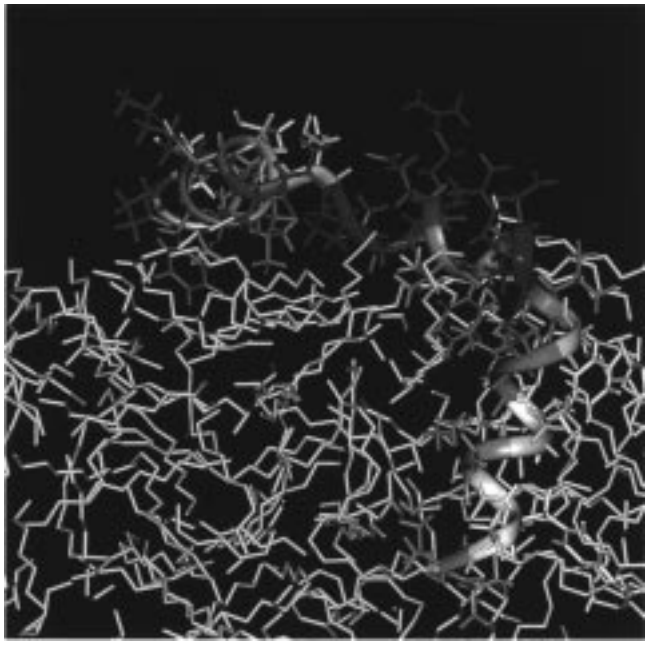

FIGURE 5: A structure of PTH1R[168−198] from the MD calculation in a water/decane simulation cell. The peptide ribbon is colored according to hydrophobicity (blue = polar, red = hydrophobic); the decane molecules are depicted in yellow and the water molecules are not displayed for clarity. The residues belonging to TM1 are to the right of the cell, embedded in the decane phase.

Table 1: Average Dihedral Angles and Standard Deviation from the Last 50 ps of Decane/Water MD Simulation

residue	ϕ	ψ
Glu^{169}	-46.7 ± 6	-37.2 ± 5
Ala^{170}	-65.7 ± 8	-45.6 ± 7
Val^{171}	-62.3 ± 5	-35.1 ± 6
Lys^{172}	-60.2 ± 6	-37.6 ± 11
Phe^{173}	-78.5 ± 11	-38.5 ± 6
Leu^{174}	-56.5 ± 9	-49.2 ± 6
Thr^{175}	-67.7 ± 9	-23.1 ± 11
Asn^{176}	-60.3 ± 11	-41.4 ± 9
Glu^{177}	-147.6 ± 11	82.5 ± 8
Thr^{178}	-76.0 ± 9	59.5 ± 19
Arg^{179}	-99.4 ± 19	-14.0 ± 10
Glu^{180}	-62.3 ± 11	-63.9 ± 11
Arg^{181}	-62.1 ± 8	-33.1 ± 9
Glu^{182}	-61.9 ± 11	-39.9 ± 12
Val^{183}	-90.8 ± 11	-20.1 ± 7
Phe^{184}	-92.4 ± 8	12.9 ± 10
Asp^{185}	-103.3 ± 9	-26.3 ± 9
Arg^{186}	-77.7 ± 7	30.7 ± 9
Leu^{187}	-43.1 ± 8	-30.5 ± 5
Gly^{188}	-65.0 ± 8	-11.9 ± 9
Met^{189}	-111.0 ± 7	-8.8 ± 9
Ile^{190}	-90.8 ± 7	-69.1 ± 6
Tyr^{191}	-55.0 ± 6	-35.2 ± 6
Thr^{192}	-50.7 ± 10	-59.3 ± 5
Val^{193}	-59.6 ± 6	-43.2 ± 6
Gly^{194}	-52.6 ± 7	-40.5 ± 13
Tyr^{196}	-70.9 ± 12	-57.3 ± 9
Ser^{197}	-77.1 ± 12	15.1 ± 28
Val^{198}	-82.9 ± 22	-27.8 ± 26

DISCUSSION

The investigation of PTH1R[168−198] was undertaken to structurally characterize a region of the human PTH1 receptor previously implicated in ligand binding (*9*). This represents an experimental approach to obtaining structural insight into membrane-embedded receptors, which as a whole, cannot generally be examined by conventional methods (X-ray crystallography, NMR spectroscopy). The choice of experimental conditions is crucial; the receptor fragment examined here, containing approximately seven residues of TM1, quickly forms a semisolid gel in water. The aqueous solution of DPC micelles provides an NMR-compatible solvent system that mimics the interface between the membrane and extracellular milieu. Indeed, all experimental results (including line broadening in the NMR spectra, TOCSY experiments with correlation behavior typical of very large molecules, and titrations with free radicals) indicate that the peptide is tightly associated with the micelle and adopts a topological orientation fully consistent with that expected for this fragment in native PTH1R.

The seven amino acids corresponding to TM1 adopt an α-helix which embeds into the hydrophobic core of the micelle. The remainder of the receptor fragment, amphipathic in nature, lies at the interface on the micelle surface with the hydrophobic face directed toward the micelle. In particular, the NMR resonances of residues Ala^{170}, Val^{171}, Phe^{173}, and Leu^{174}, on the hydrophobic face of the N-terminal helix, are significantly broadened by the addition of 5-doxylstearic acid and therefore lie at the micelle surface. In contrast, Glu^{169}, Lys^{172}, and Asn^{176}, making up the hydrophilic face of the N-terminal helix, are unaffected and likely exposed to the solvent.

The H_2O/decane box used for the MD simulations reproduces the biphase character of the aqueous micellular solution. The decane molecules mimic the hydrophobic phase created by the alkylic chains of the DPC molecules. In this simulation system, the correct description of the charged interface, created by the phosphate and choline groups of the DPC, is sacrificed for simplicity and computational speed, which in turn allows for extended simulations starting from different orientations. The goal of the simulations is further refinement of the receptor and verification of the energetic stability of the DG-generated structures in an environment similar to that used for the NMR experiments. Additionally, the simulations provided further evidence for the preferred partitioning of the molecule between the hydrophobic and hydrophilic phases. Despite the fact that no constraint on the location of the peptide within the two-phase box was applied, the TM1 helix was always found embedded in the decane phase, approximately perpendicular to the interface. The remaining peptide chain prefers to occupy a position at the interface, allowing for optimal interactions of the two amphipathic helices with the solvents. This topological arrangement is in complete accord with the experimental results and fully consistent with that expected for this region in the intact receptor.

While the placement and relative arrangement of the seven TM helices in G-protein coupled receptors is relatively well understood from the studies of rhodopsin and bacteriorhodopsin (*11*) and other membrane embedded proteins (chiefly the bacterial reaction center), little is known about the structure of the intra- and extracellular termini and loops. The determination of the structural elements of the loops and termini would afford important insight into the biomolecular interactions of the receptor with the G-protein (intracellular domain) (*40*−*42*) and with the hormone-ligand (extracellular domain) (*43*, *44*). These studies would reveal the determinants which confer the specificity of ligand-

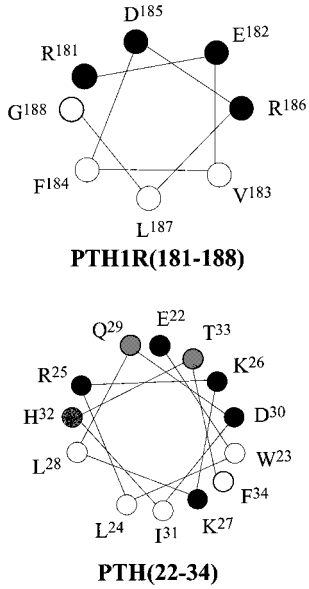

FIGURE 6: Helical wheel diagrams depicting the amphipathic α-helical regions of PTH1R[168−198] (top) and PTH (bottom) which have been shown to associate with the micelle surface. The hydrophilic residues are filled, the hydrophobic residues are open.

recognition and signal transduction. In this study, the conformational features and topological orientation of an extracellular fragment of the PTH1R, associated with ligand binding, are reported.

The NMR-derived structure of PTH(1−34), a fully potent fragment of PTH, in the presence of DPC micelles was recently described (*10*). The results indicate that the C-terminus, including the binding domain [residues 25−34 (*8*)], adopts an amphipathic α-helix, which lies on the surface of the lipid. The current finding that the contact domain of PTH1R, residues Phe^{173}−Met^{189}, also folds into an amphipathic α-helix and lies on the lipid surface suggests a possible interaction between ligand and receptor. We propose that the initial binding event involves the amphipathic α-helices of the ligand (consisting of residues 19−33 of PTH) (*10*, *45*) and receptor (residues 181−189 and possibly, the N-terminal helix, residues 169−176), all of which have been experimentally verified to readily associate with the membrane surface. Helical wheel diagrams of these regions of PTH and receptor fragment are depicted in Figure 6. A theory that the recognition of peptide hormones by membrane bound receptors is preceded by nonspecific preadsorption on the target cell membrane has been described (*46*, *47*). The theory proposes that the hydrophobic adsorption is followed by a random, two-dimensional diffusion leading to lateral collisions of the folded structure (membrane-induced structure) of the peptide hormone with the receptor. If this is the case, the amino acids exposed to the solution, available for helix−helix interaction, would be crucial for binding. The hydrophilic face of the receptor helix includes Glu^{177}, Arg^{179}, Arg^{181}, Glu^{182}, Asp^{185}, and Arg^{186}. The charges of these amino acids readily avail themselves to Columbic interactions with the complementarily charged residues of the amphipathic helix of the ligand, including Arg^{25}, Lys^{26}, Lys^{27}, and Asp^{30}. These helix−helix interactions provide the affinity and specificity associated with ligand binding. To test this model, the importance of each of these residues, individually and pairwise, for ligand binding must be examined. It is important to note that the receptor fragment examined here probably constitutes only one domain of the ligand binding pocket and the role of the remainder of the N-terminus, as well as the extracellular loops, in the formation of the ligand−receptor complex will have to be determined.

REFERENCES

1. Suva, L. J., Winslow, G. A., Wettenhall, R. E. H., Hammond, R. G. G., Moseley, J. M., Diefenback-Jagger, H., Rodda, C. P., Kemp, B. E., Rodriguez, H., Chen, E. Y., Hundson, P. J., and Martin, T. J. (1987) *Science 237*, 893−896.
2. Jüppner, H., Abou-Samra, A. B., Freeman, M. W., Kong, X. F., Schipani, F., Richards, J., Kolakowski, L. F. J., Hock, J., Potts, J. T., Jr, and Kronenberg, H. M. (1991) *Science 254*, 1024−1026.
3. Segre, g. V., and Goldring, S. R. (1993) *Trends Endocrinol. Metab. 4*, 309−314.
4. Bergwitz, C., Gardella, T. J., Flannery, M. R., Potts, J. T. j., Kronenberg, H. M., Goldring, S. R., and Juppner, H. (1996) *J. Biol. Chem. 271*, 26469−26472.
5. Lee, C., Gardella, T. J., Abou-Samra, A. B., Nussbaum, S. R., Segre, G. V., Potts, J. T., Jr., Kronenberg, H. M., and Jüppner, H. (1994) *Endocrinology 135*, 1488−1495.
6. Urena, P., Abou Samra, A. B., Jüppner, H., Kong, X. F., Lee, K., Bringhurst, F. R., and Segre, G. V. (1994) *Ann. Endocrinol. (Paris) 55* (54O), 133−141.
7. Rosenblatt, M., Callahan, E. N., Mahaffey, J. E., Pont, A., and Potts, J. T., Jr. (1977) *J. Biol. Chem. 252*, 5847−5851.
8. Nussbaum, S. R., Rosenblatt, M., and Potts, J. T., Jr. (1980) *J. Biol. Chem. 255*, 10183−10187.
9. Zhou, A. T., Bessalle, R., Bisello, A., Nakamoto, C., Rosenblatt, M., Suva, L. J., and Chorev, M. (1997) *Proc. Natl. Acad. Sci. U.S.A. 94*, 3644−3649.
10. Pellegrini, M., Royo, M., Rosenblatt, M., Chorev, M., and Mierke, D. F. (1998) *J. Biol. Chem. 273*, 10420−10427.
11. Pebay Peyroula, E., Rummel, G., Rosenbusch, J. P., and Landau, E. M. (1997) *Science 277*, 1676−1681.
12. Schertler, G. F., Villa, C., and Henderson, R. (1993) *Nature 362*, 770−772.
13. Altshul, S. F., Gish, W., Miller, W., Myers, E. W., and Lipman, D. J. (1990) *J. Mol. Biol. 215*, 403−410.
14. van Buuren, A. R., Marrink, S., and Berendsen, H. J. C. (1993) *J. Phys. Chem. 97*, 9206−9216.
15. Nakamoto, C., Behar, V., Chin, K. R., Adams, A. E., Suva, L. J., Rosenblatt, M., and Chorev, M. (1995) *Biochemistry 34*, 10546−10552.
16. Rance, M., Sørensen, O. W., Bodenhausen, G., Wagner, G., Ernst, R. R., and Wüthrich, K. (1983) *Biochem. Biophys. Res. Commun. 117*, 458−479.
17. Braunschweiler, L., and Ernst, R. R. (1983) *J. Magn. Reson. 53*, 521−528.
18. Bax, A., and Davis, D. G. (1985) *J. Magn. Reson. 65*, 355−360.
19. Jeener, J., Meier, B. H., Bachmann, P., and Ernst, R. R. (1979) *J. Chem. Phys. 71*, 4546−4553.
20. Macura, S., Huang, Y., Suter, D., and Ernst, R. R. (1981) *J. Magn. Reson. 43*, 259−281.
21. Plateau, P., and Gueron, M. (1982) *J. Am. Chem. Soc. 104*, 7310−7311.
22. Wüthrich, K. (1986) *NMR of Proteins and Nucleic acids*, Wiley, New York.
23. Cavanagh, J., Fairbrother, W. J., Palmer, A. G., and Skelton, N. J. (1996) *Protein NMR Spectroscopy, Principle and Practice*, Academic Press, New York.
24. Weber, P. L., Morrison, R., and Hare, D. (1988) *J. Mol. Biol. 204*, 483−487.
25. Havel, T. F. (1991) *Prog. Biophys. Mol. Biol. 56*, 43−78.
26. Kaptein, R., Boelens, R., Scheek, R. M., and van Gunsteren, W. F. (1988) *Biochemistry 27*, 5389−5395.
27. Mierke, D. F., Geyer, A., and Kessler, H. (1994) *Int. J. Pept. Protein Res. 44*, 325−331.

28. Jahnke, W., Mierke, D. F., Beress, L., and Kessler. (1994) *J. Mol. Biol. 240*, 445−458.
29. van der Spoel, D., van Buuren, A. R., Apol, E., Meulenhoff, P. J., Tieleman, D. p., Sijbers, A. L. T. M., van Drunen, R., and Berendsen, H. J. C. (1996) *Gromacs User Manual*, University of Groningen.
30. Ryckaert, J. P., and Bellemans, A. (1978) *Faraday Discuss. Chem. Soc. 66*, 95.
31. Berendsen, H. J. C., Postma, J. P. M., van Gunsteren, W. F., and Hermans, J. (1981) *Intermolecular forces*, pp 331−342, D. Reidel Publishing Co., Dodrecht.
32. Miyamoto, S., and Kollman, P. A. (1992) *J. Comput. Chem. 13*, 952−962.
33. Berendsen, H. J. C., Postma, J. P. M., DiNola, A., and Haak, J. R. (1984) *J. Chem. Phys. 81*, 3684−3690.
34. McDonnel, P. A., and Opella, S. J. (1993) *J. Magn. Reson. B 102*, 120−125.
35. Kallick, D. A., Tesmer, M. R., Watts, C. R., and Li, C. (1995) *J. Magn. Reson. B 109*, 60−65.
36. Pastore, A., and Saudek, V. (1990) *J. Magn. Reson. 90*, 165−176.
37. Wishart, D. S., Sykes, B. D., and Richards, F. M. (1992) *Biochemistry 31*, 1647−1651.
38. Brown, L. R., Bösch, C., and Wüthrich, K. (1981) *Biochim. Biophys. Acta 642*, 296−312.
39. van de Ven, F. J. M., van Os, J. W. M., Aelen, J. M. A., Wymenga, S. S., Remerowsky, M. L., Konings, R. N. H., and Hilbers, C. W. (1993) *Biochemistry 32*, 8322−8328.
40. Pellegrini, M., Royo, M., Chorev, M., and Mierke, D. F. (1996) *J. Pept. Sci. 40*, 653−666.
41. Mierke, D. F., Royo, M., Pellegrini, M., Sun, H., and Chorev, M. (1996) *J. Am. Chem. Soc. 118*, 8998−9004.
42. Yeagle, P. L., Alderfer, J. L., Salloum, A. C., Ali, L., and Albert, A. D. (1997) *Biochemistry 36*, 3864−3869.
43. Pervushin, K. V., Yu, V., Popov, A. I., Musina, L. Y., and Arseniev, A. S. (1994) *Eur. J. Biochem. 219*, 571−583.
44. Pashkov, V. S., Balashova, T. A., Zhemaeva, L. V., Sikilnda, N. N., Kutuzov, M. A., Abdulaev, N. G., and Arseniev, A. S. (1996) *FEBS Lett. 381*, 119−122.
45. Mierke, D. F., Maretto, S., Schievano, E., DeLuca, D., Bisello, A., Mammi, S., Rosenblatt, M., Peggion, E., and Chorev, M. (1997) *Biochemistry 36*, 10372−10383.
46. Schwyzer, R. (1986) *Natural Products and Biological Activities*, Tokio Press and Elsevier, Tokio.
47. Moroder, L., Romano, R., Guba, W., Mierke, D. F., Kessler, H., Delporte, C., Winand, J., and Christophe, J. (1993) *Biochemistry 32*, 13551−13559.

BI981265H